



Concentration and distribution of lithium in catchment sediments of China: Conclusions from the China Geochemical Baselines project

Hanliang Liu, Xueqiu Wang*, Bimin Zhang, Wei Wang, Zhixuan Han, Qinghua Chi, Jian Zhou, Lanshi Nie, Shanfa Xu, Wensheng Yao, Dongsheng Liu, Qingqing Liu, Jian Liu

Key Laboratory of Geochemical Exploration, Institute of Geophysical and Geochemical Exploration, Chinese Academy of Geological Sciences, Langfang, Hebei 065000, China
UNESCO International Centre on Global-scale Geochemistry, Langfang, Hebei 065000, China

ARTICLE INFO

Keywords:

Lithium (Li)
Concentration and distribution
China Geochemical Baselines project
Catchment sediment

ABSTRACT

With the ever-increasing demand for lithium (Li), understanding its concentration and distribution in the pedosphere is essential for alleviating the Li shortage in China. The China Geochemical Baselines (CGB) project, which commenced in 2008, provided comparable global-scale geochemical Li data. A total of 3394 top (0–25 cm) and 3394 deep (below 100 cm) catchment sediment samples were collected. The range of Li concentrations in the top and deep samples were 5.37–400 mg·kg⁻¹ with a median value of 30.0 mg·kg⁻¹, and 5.27–400 mg·kg⁻¹ with a median value of 28.6 mg·kg⁻¹, respectively. The Li concentrations in the top and deep catchment sediments of China showed large variations across regions but only mild variability across profiles. Parent rock, especially granite, predominantly governed the Li distribution in the catchment sediments of China. Landscapes, mineralization and weathering played regional-scale roles. Macroscopically, the low background area (< P25) was mainly distributed in the northern margin of the North China craton, and Hainan Island, and the high background area (> P75) was mainly distributed in the Altay, South China, Sanjiang and Himalayan orogenic belts, and the Yangtze craton. Based on a cumulative frequency of the 85th percentile, a total of 16 geochemical anomalies were identified, and eight important prospective Li resources were selected where many world-renowned Li deposits were formed.

1. Introduction

Lithium (Li) is the lightest metal and the least dense solid element. Due to its physical and chemical properties, Li and its compounds have highly diverse industrial applications. According to Jaskula (2017), the global end-use markets for Li are estimated as follows: batteries, 39%; ceramics and glass, 30%; lubricating greases, 8%; continuous casting mold flux powders and polymer production, 5% each; air treatment, 3%; and other uses, 10%. Lithium plays an increasingly important role in emerging clean technologies (Gil-Alana and Monge, 2019). China's existing Li supply is highly dependent on foreign countries. In 2017, 80% of Li was imported including 89,200 tons of Li pyroxene from Australia, accounting for 57%, and about 35,600 tons of salt lake Li from South America, accounting for 23% (Ma and Li, 2018). The development and utilization of Li resources are included in the “13th Five-Year Plan” as part of China's national strategy. Hence, understanding the concentration and distribution of Li in the pedosphere is necessary

to alleviate the Li shortage in China. However, comprehensive knowledge of Li in the lithosphere and pedosphere, especially on the global-scale, is still deficient.

Recently, an ultra-low density geochemical mapping project, the China Geochemical Baselines (CGB) project, was completed which documented the abundance and spatial distribution of 76 elements throughout mainland China (Wang et al., 2015). The CGB project was conducted as a part of the International Union of Geological Sciences/International Association of Geochemistry Task Group on Global Geochemical Baselines (Darnley et al., 1995; Smith et al., 2012). Both catchment sediment and rock samples were taken during the CGB project. Seventy-six elements were determined under strict laboratory analytical quality controls, which provided information about concentrations and distribution of elements at the global scale (Wang, 2012). For example, the concentrations and distribution of Hg, Pb, and Mo were reported from the CGB project data (Wang et al., 2015, 2019; Lin et al., 2019).

* Corresponding author at: Key Laboratory of Geochemical Exploration, Institute of Geophysical and Geochemical Exploration (IGGE), Chinese Academy of Geological Sciences, Langfang, Hebei 065000, China.

E-mail address: wangxueqiu@igge.cn (X. Wang).

<https://doi.org/10.1016/j.gexplo.2020.106540>

Received 19 November 2019; Received in revised form 23 March 2020; Accepted 28 March 2020

Available online 31 March 2020

0375-6742/ © 2020 Elsevier B.V. All rights reserved.

To interpret continental-scale geochemical maps, factors must be taken into account, including the landscape, geology (parent rock types), vegetation coverage, climate, and human activities, such as land use, population and traffic density, and the distribution of major industries (Reimann et al., 2012). However, it is far beyond the scope of this paper to cover all the aspects. Instead, this study uses the CGB project data to 1) present the concentration and spatial distribution of Li, 2) investigate influences such as geological background (parent rock types), landscape, and mineralization; and 3) identify eight important prospective Li resources.

2. Materials and methods

2.1. Sampling

The CGB project aimed to document the concentration and spatial distribution of nearly all naturally occurring chemical elements, including Li, throughout China. Catchment sediments were selected as the sampling media because they can provide high-resolution and comparable nationwide baseline data (Salminen and Tarvainen, 1997; Xie and Cheng, 1997; Caritat et al., 2009, 2018; Wang et al., 2015). Two sampling sites were allocated in each CGB grid cell of 1° (longitude) \times $40'$ (latitude), which is approximately equal to $80 \text{ km} \times 80 \text{ km}$ (Darnley et al., 1995; Wang et al., 2015). Top samples were typically collected from the soil A-horizon at depths of 0–25 cm, while deep samples were collected from depths $> 100 \text{ cm}$ or the deepest possible part of the C-horizon. Each sample was composited from three samples collected at the vertices of an equilateral triangle with 50 m sides. In total, 3394 top and 3394 deep samples were collected from 1500 CGB grid cells at an average density of 1 site per 3000 km^2 , which covered about 94% of China's land area (Fig. 1). Rock samples were simultaneously collected from each CGB grid cell, which typically represented the main types of rocks, including sedimentary, igneous and metamorphic rocks for different geological times (Wang, 2012;

Wang et al., 2015). A total of 2077 acidic rock samples were collected in 1000 CGB grid cells where exposed bedrock was available (Fig. 1). The weight of each sample was $> 5 \text{ kg}$, and the sampling methods are described in greater detail in Wang et al. (2015).

2.2. Sample preparation and analysis

All catchment sediment samples were air-dried either in a room or under shade, without exposure to sunlight, and sieved through a 2 mm nylon mesh screen. Rock samples were crushed to sizes $< 2 \text{ mm}$ using a jaw crusher. All samples were subsequently ground to $< 74 \mu\text{m}$ (200 mesh) in an agate mill. Samples were analyzed at the Institute of Geophysical and Geochemical Exploration (IGGE), Chinese Academy of Geological Sciences (CAGS). The analytical scheme and quality monitoring system used to analyze the 76 elements were developed in the CGB project (Zhang et al., 2012; Wang et al., 2015).

An aliquot (0.250 g) was placed into a 25 ml test tube to which HF (10 ml), HNO_3 (5 ml), HClO_4 (2 ml), and aqua regia (8 ml) were added. The test tube was heated in a boiling water bath for 1 h and shaken once during decomposition. After cooling, 1 ml of the supernatant was diluted to 10 ml by adding 2% HNO_3 solution. This solution was used to determine the total Li concentration by inductively coupled plasma mass spectrometry (ICP-MS) (Zhang et al., 2012). The detection limit was $1 \text{ mg}\cdot\text{kg}^{-1}$, and the reportable rate was 100%.

The standardized quality control procedures were as follows: 1) field training for all sampling participants; 2) field sampling checking by randomly selecting $> 5\%$ of the sampling sites; 3) collecting 3% field duplicate samples; 4) blank insertion of 10% laboratory replicate samples; and 5) insertion of four standard reference materials into each batch of 50 routine samples (Zhang et al., 2012; Wang et al., 2015; Wang et al., 2019; Caritat et al., 2018). The pass percentage rates required for the national standard reference materials, laboratory replicate samples and field duplicates were 100%, 100% and 98.6%, respectively. The CGB project obtained high-quality Li data.

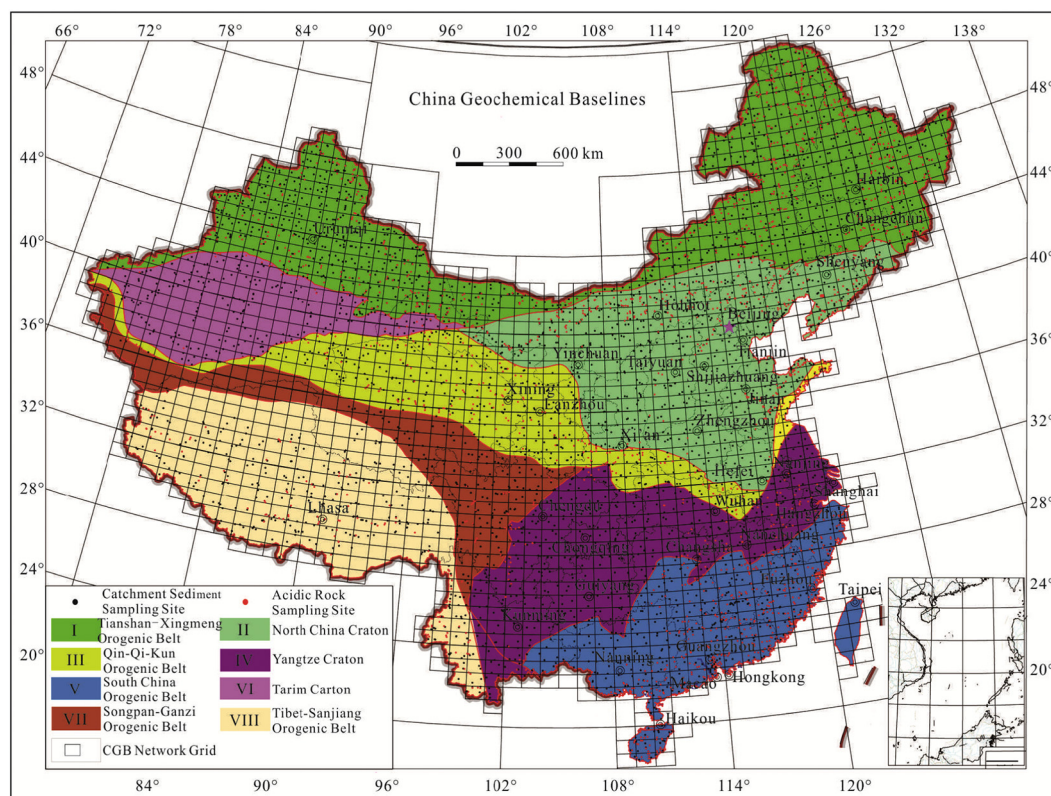


Fig. 1. Sampling sites and tectonic units map of the China Geochemical Baselines (CGB) project, modified from Wang et al. (2015).

Table 1Statistical summary of Li analytical results ($\text{mg}\cdot\text{kg}^{-1}$) in the top and deep catchment sediment samples from the CGB project.

Sample type	Num.	Min.	P2.5	P25	P50	P75	P85	P97.5	Max.	AM	GM
Top	3394	5.37	11.2	22.7	30.0	37.6	42.9	62.3	400	31.6	28.8
Deep	3394	5.27	9.55	20.7	28.6	37.5	42.8	63.7	400	30.6	27.4

Notation: Num. = Number of samples; P = Percentile (P50 = Median); Min. = Minimum; Max. = Maximum; AM = Arithmetic mean; GM = Geometric mean.

3. Results and discussion

3.1. Concentration of Li in China

A summary of the statistics of the Li concentrations determined by the CGB project is shown in Table 1. The Li concentrations in the top samples ranged from 5.37 to 400 $\text{mg}\cdot\text{kg}^{-1}$, with a median of 30.0 $\text{mg}\cdot\text{kg}^{-1}$, arithmetic mean of 31.6 $\text{mg}\cdot\text{kg}^{-1}$, and geometric mean of 28.8 $\text{mg}\cdot\text{kg}^{-1}$; Li concentrations in the deep samples ranged from 5.27 to 400 $\text{mg}\cdot\text{kg}^{-1}$, with a median of 28.6 $\text{mg}\cdot\text{kg}^{-1}$, arithmetic mean of 30.6 $\text{mg}\cdot\text{kg}^{-1}$, and geometric mean of 27.4 $\text{mg}\cdot\text{kg}^{-1}$. The observed element concentrations within different soil horizons substantially shifted relative to their sources in a relatively short span of geological time due to complex chemical reactions. In addition, the deeper soil horizon is typically used to reflect the natural, geogenic element pool and regional variations (Reimann et al., 2007). This general similarity of Li in the top and deep samples indicates that they may have experienced similar and consistent formation processes. The Li concentrations in the top samples were slightly higher than those in the deep samples, mainly due to modern anthropogenic additions in regions where long-term mining and industrial activities have occurred. In addition, the arithmetic mean (AM), the geometric mean (GM), and the median were arranged in the sequence: $\text{AM} > \text{Median} \approx \text{GM}$. This shows that the Li concentrations in the top and deep samples followed a log-normal distribution (Reimann et al., 2008), which was also shown by the histograms and boxplots (Fig. 2).

The Li concentrations present in various loose sediments throughout China are summarized in Table 2. The statistical parameters (median, arithmetic mean, and geometric mean) of this study were slightly lower than, but comparable to, those of previous studies, implying that the global-scale geochemical mapping method is suitable for rapidly gathering an overview of geochemical information in mega-regions. The Li

concentrations in the continental crust and rocks are summarized in Table 3. The Li concentration in the top and deep samples was higher than those in the continental crust, which varied from 13 to 20 $\text{mg}\cdot\text{kg}^{-1}$. This indicates that Li was enriched during soil formation. In terms of rock types, acidic rocks were present in the highest concentrations in igneous rocks, followed by intermediate rocks, basic rocks, and ultramafic rocks. Shale was the highest in sedimentary rocks, followed by sandstone and carbonate rocks (Table 3).

3.2. Concentration of Li in China's tectonic units

Mainland China is geologically divided into eight tectonic units (Fig. 1, Ren et al., 1999; Wang et al., 2015): I: Tianshan-Xingmeng orogenic belt; II: North China craton; III: Qin-Qi-Kun orogenic belt; IV: Yangtze craton; V: South China orogenic belt; VI: Tarim craton; VII: Songpan-Ganzi orogenic belt; and VIII: Tibet-Sanjiang orogenic belt (Ren et al., 1999). China is located in a unique tectonic setting where the Paleo-Asian Ocean, Tethyan, and western Pacific domains meet in a triangular framework. China's continental crust is a mosaic of cratonic blocks and orogenic belts and contains small cratons and terranes with various tectonic settings. They have diverse origins and complex histories of amalgamation and have often suffered repeated reworking after multiple amalgamations (Zheng et al., 2013).

Table 4 shows the statistical summary of the Li concentrations present in the top and deep catchment sediment samples from different tectonic units of China, and Fig. 3 shows the Li statistical distribution as boxplots. The median values of top samples were ranked as follows: Songpan-Ganzi orogenic belt (36.0 $\text{mg}\cdot\text{kg}^{-1}$) > Yangtze craton (35.8 $\text{mg}\cdot\text{kg}^{-1}$) > Tibet-Sanjiang orogenic belt (33.5 $\text{mg}\cdot\text{kg}^{-1}$) > South China orogenic belt (32.5 $\text{mg}\cdot\text{kg}^{-1}$) > China (30.0 $\text{mg}\cdot\text{kg}^{-1}$) > Qin-Qi-Kun orogenic belt (29.7 $\text{mg}\cdot\text{kg}^{-1}$) > Tianshan-Xingmeng orogenic belt

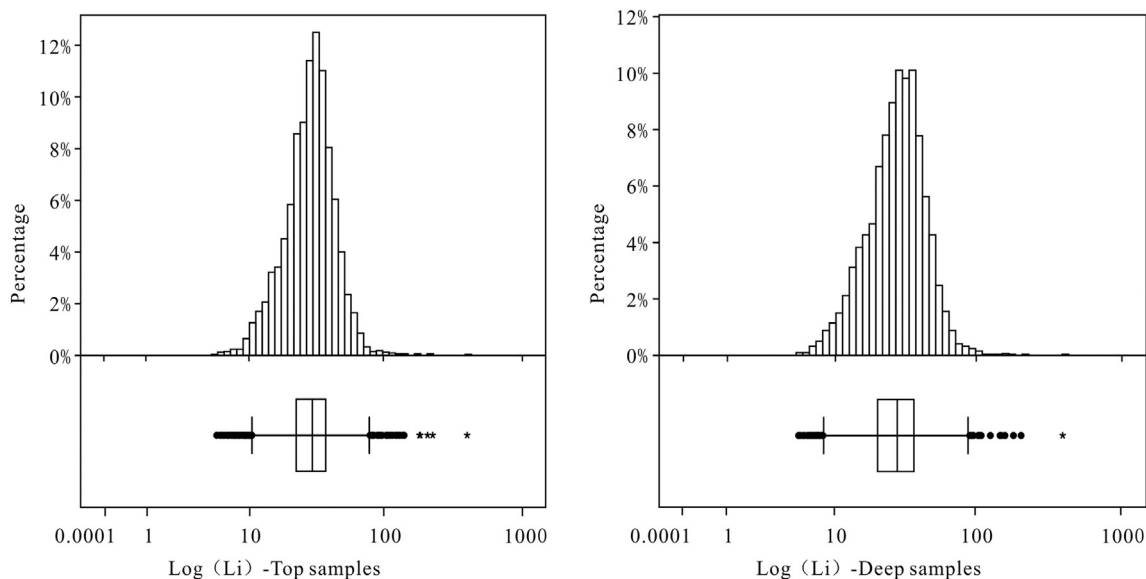


Fig. 2. Histograms and boxplots displaying the statistical Li distribution ($\text{mg}\cdot\text{kg}^{-1}$) in top and deep samples from the CGB data. The box length represents the interquartile range and contains the median. ‘*’: Values between 1.5 and 3 times the box length from either edge of the box; ‘**’: Values > 3 times the box length from either edge of the box.

Table 2
Lithium concentrations ($\text{mg}\cdot\text{kg}^{-1}$) in various loose sediments throughout China.

Soil type	Sample number	Parameter	Li concentration	Reference
Topsoil	4095	M	31	CNECM (1990)
		AM	32	
		GM	29	
Floodplain sediments	529	M	35	Xie and Cheng (2001)
Stream sediments	44,422	M	32	Chi and Yan (2007)
		AM	34	
		GM	31	

Notation: M = Median; AM = Arithmetic mean; GM = Geometric mean.

Table 3
Lithium concentrations ($\text{mg}\cdot\text{kg}^{-1}$) in continental crust and rocks.

Type	Li	Reference	
Crust	Continental crust	20 Taylor, 1964	
	Continental crust	13 Taylor and McLennan, 1985	
	Continental crust	18 Wedepohl, 1995	
	Continental crust	16 Rudnick and Gao, 2003	
	Continental crust in the eastern part of China	17 Yan and Chi, 2005	
	Rock	Acidic rock in China	19 Yan and Chi, 2005
		Granite in China	19 Yan and Chi, 2005
Granite in China		21 Shi et al., 2005	
Rhyolite in China		15 Yan and Chi, 2005	
Intermediate rock in China		13 Chi and Yan, 2007	
Diorite in China		12.6 Yan and Chi, 2005	
Andesite in China		14 Yan and Chi, 2005	
Basic rock in China		11 Yan and Chi, 2005	
Gabbros in China		10 Yan and Chi, 2005	
Diabase in China		11 Yan and Chi, 2005	
Basalt in China		12 Yan and Chi, 2005	
Ultramafic rock in China		4 Yan and Chi, 2005	
Sandstone in eastern China		25 Yan and Chi, 2005	
Shale in eastern China		38 Yan and Chi, 2005	
Carbonate rock in eastern China		10.5 Yan and Chi, 2005	
Limestone in eastern China		9.5 Yan and Chi, 2005	
Dolomite in eastern China		8 Yan and Chi, 2005	
Siliceous rock in eastern China		11 Yan and Chi, 2005	
Slate in eastern China		35 Yan and Chi, 2005	
Phyllite in eastern China		33 Yan and Chi, 2005	
Schist in eastern China	28 Yan and Chi, 2005		
Gneiss in eastern China	14 Yan and Chi, 2005		
Marble in eastern China	8.6 Yan and Chi, 2005		

($27.6 \text{ mg}\cdot\text{kg}^{-1}$) > Tarim craton ($27.2 \text{ mg}\cdot\text{kg}^{-1}$) > North China craton ($25.8 \text{ mg}\cdot\text{kg}^{-1}$). The median values of the deep samples were ranked as follows: Yangtze craton ($36.3 \text{ mg}\cdot\text{kg}^{-1}$) > Songpan-Ganzi orogenic belt ($36.1 \text{ mg}\cdot\text{kg}^{-1}$) > South China orogenic belt ($34.4 \text{ mg}\cdot\text{kg}^{-1}$) > Tibet-Sanjiang orogenic belt ($33.2 \text{ mg}\cdot\text{kg}^{-1}$) > China ($28.6 \text{ mg}\cdot\text{kg}^{-1}$) > Qin-Qi-Kun orogenic belt ($28.2 \text{ mg}\cdot\text{kg}^{-1}$) > Tarim craton ($25.5 \text{ mg}\cdot\text{kg}^{-1}$) > North China craton ($24.6 \text{ mg}\cdot\text{kg}^{-1}$) > Tianshan-Xingmeng orogenic belt ($23.6 \text{ mg}\cdot\text{kg}^{-1}$). Fig. 3 shows that for all geotectonic units, the top and deep samples shared similar data structures. The tectonic units with higher Li concentration included the Songpan-Ganzi orogenic belt, the Yangtze craton, the Tibet-Sanjiang orogenic belt, and the South China orogenic belt. Large exposed granite rocks contribute to Li enrichment in the Songpan-Ganzi, Tibet-Sanjiang and South China orogenic belts. At the same time, large-scale Li deposits are also developed here, such as: Jiajika, Lijiagou, Ke'eryin, Guanyinqiao, Yichun 414, Jianfengling, Tongan, Zhengchong, Xikeng (Table 6, Fig. 6). The high Li content of the Yangtze craton may be related to the widely developed black shale extending along a 1600 km belt from the Yunnan province in the south-southwest to the Zhejiang province (Mao et al., 2002; Zheng et al., 2013).

3.3. Concentration of Li in China's geomorphologic landscapes

China occupies an area from latitude and longitude values of $18\text{--}54^\circ\text{N}$ and $135\text{--}173^\circ\text{E}$, respectively. The geomorphology of Chinese landscapes is highly diverse (Fig. 4; Wang and Zuo, 2010), with its Eastern and northeastern areas dominated by hilly or low-mountainous areas, alluvial plains, and forested land. Northern and Northwest China include arid desert terrains, including desert basins, the gobi desert,

Table 4
Statistical summary of Li ($\text{mg}\cdot\text{kg}^{-1}$) in top and deep catchment sediment samples in China's geological tectonic units.

Tectonic unit	Sample type	Num.	Min.	P2.5	P25	P50	P75	P85	P97.5	Max.	AM	GM
China	Top	3394	5.37	11.2	22.7	30.0	37.6	42.9	62.3	400	31.6	28.8
	Deep	3394	5.27	9.55	20.7	28.6	37.5	42.8	63.7	400	30.6	27.4
I	Top	922	5.37	10.5	20.6	27.6	34.6	38.9	55.6	400	29.2	26.3
	Deep	922	5.37	8.78	16.6	23.6	32.0	37.2	57.5	400	26.4	23.1
II	Top	613	5.74	9.81	18.2	25.8	32.5	36.1	46.5	62.8	26.0	24.0
	Deep	613	5.42	8.48	15.7	24.6	31.8	36.4	48.7	62.8	25.1	22.6
III	Top	350	9.57	12.4	23.0	29.7	35.2	38.7	52.9	70.4	29.5	27.7
	Deep	350	5.27	11.3	21.9	28.2	35.1	39.1	52.8	92.6	29.1	27.1
IV	Top	399	7.35	16.1	28.7	35.8	42.7	48.1	67.1	226	37.9	35.3
	Deep	399	7.35	15.0	29.0	36.3	43.4	49.0	70.8	127	37.8	35.3
V	Top	351	5.85	11.2	23.3	32.5	43.8	50.3	70.3	126	34.7	31.0
	Deep	351	7.11	12.4	24.4	34.4	46.4	53.4	76.6	97.3	36.7	33.0
VI	Top	209	6.12	15.8	21.6	27.2	33.8	39.4	52.4	61.5	28.9	27.4
	Deep	209	8.31	14.0	21.1	25.5	31.4	35.2	51.2	58.6	27.2	25.8
VII	Top	202	15.6	20.6	29.9	36.0	42.2	47.2	60.7	68.0	37.1	35.7
	Deep	202	14.9	19.7	29.7	36.1	42.0	47.2	62.6	70.8	37.0	35.6
VIII	Top	348	13.2	17.2	26.6	33.5	46.6	51.6	74.0	207	37.9	34.9
	Deep	348	8.62	15.5	25.3	33.2	44.2	51.6	75.5	207	37.0	33.7

Notation: Num. = Number of samples; P = Percentile (P50 = Median); Min. = Minimum; Max. = Maximum; AM = Arithmetic mean; GM = Geometric mean; China – all samples; I – Tianshan-Xingmeng orogenic belt; II – North China craton; III – Qin-Qi-Kun orogenic belt; IV – Yangtze craton; V – South China orogenic belt; VI – Tarim craton; VII – Songpan-Ganzi orogenic belt; VIII – Tibet-Sanjiang orogenic belt.

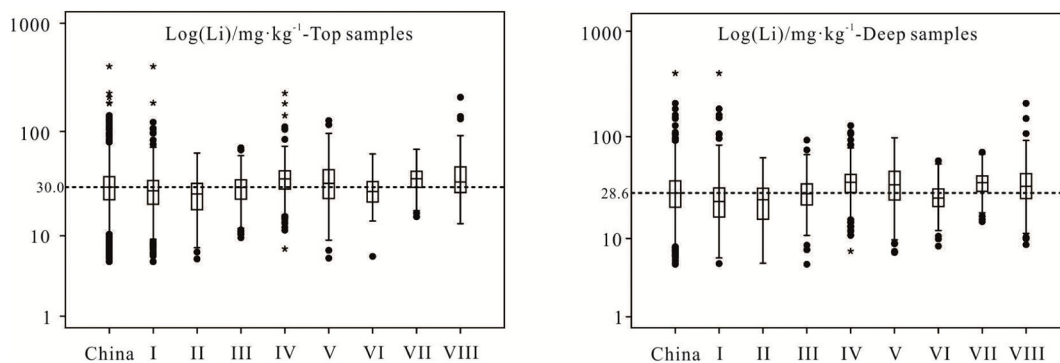


Fig. 3. Boxplots showing the Li ($\text{mg}\cdot\text{kg}^{-1}$) variation in top and deep catchment sediment samples in different tectonic units of China. The dotted lines at 30.0 and 28.6 $\text{mg}\cdot\text{kg}^{-1}$ Li mark the median concentrations of the top and deep catchment sediment samples in all of China, respectively. Notation: China – all samples; I – Tianshan-Xingmeng orogenic belt; II – North China craton; III – Qin-Qi-Kun orogenic belt; IV –Yangtze craton; V – South China orogenic belt; VI – Tarim craton; VII – Songpan-Ganzi orogenic belt; VIII – Tibet-Sanjiang orogenic belt.

semi-desert grasslands, and loess plateaus. High mountains, most notably the Himalayas, dominate southwestern China (Wang et al., 2015).

Statistics describing the Li concentrations for ten landscape types were compiled and plotted (Table 5, Fig. 5). The median values of the top samples were ranked as follows: Karst (33.4 $\text{mg}\cdot\text{kg}^{-1}$) > High mountain (32.9 $\text{mg}\cdot\text{kg}^{-1}$) > Alluvium plain (30.3 $\text{mg}\cdot\text{kg}^{-1}$) > Cold swamp (30.1 $\text{mg}\cdot\text{kg}^{-1}$) > Hill (30.0 $\text{mg}\cdot\text{kg}^{-1}$) = China (30.0 $\text{mg}\cdot\text{kg}^{-1}$) > Swamp and forest (29.8 $\text{mg}\cdot\text{kg}^{-1}$) > Loess (29.5 $\text{mg}\cdot\text{kg}^{-1}$) > Gobi desert (27.0 $\text{mg}\cdot\text{kg}^{-1}$) > Desert basin (22.9 $\text{mg}\cdot\text{kg}^{-1}$) > Semi-desert grassland (21.3 $\text{mg}\cdot\text{kg}^{-1}$). The median values of the deep samples were ranked as follows: Karst (35.4 $\text{mg}\cdot\text{kg}^{-1}$) > High mountain (32.5 $\text{mg}\cdot\text{kg}^{-1}$) > Cold swamp (30.6 $\text{mg}\cdot\text{kg}^{-1}$) > Alluvium plain (30.4 $\text{mg}\cdot\text{kg}^{-1}$) > Hill (29.5 $\text{mg}\cdot\text{kg}^{-1}$) > China (28.6 $\text{mg}\cdot\text{kg}^{-1}$) > Swamp and forest (27.8 $\text{mg}\cdot\text{kg}^{-1}$) > Loess (27.3 $\text{mg}\cdot\text{kg}^{-1}$) > Desert basin (21.4 $\text{mg}\cdot\text{kg}^{-1}$) > Gobi desert (21.3 $\text{mg}\cdot\text{kg}^{-1}$) > Semi-desert

grassland (19.8 $\text{mg}\cdot\text{kg}^{-1}$). The top samples generally displayed a similar data structure to the deep samples. Regardless of which data was selected, the median Li values were low in the desert basin, gobi desert, and semi-desert grassland. This may have been because the presence of quartz-rich aeolian sand led to a decrease in the clay content, which the soil Li content is strongly correlated with (Ashry, 1973; Anderson et al., 1988). In contrast, the karst landscape had the highest median values in the top and deep samples, which is confounding because the carbonate rocks had a low Li abundance of around 10.5 $\text{mg}\cdot\text{kg}^{-1}$ (Table 3, Yan and Chi, 2005). Re-examining the spatial distribution of the karst showed that black shales enriched in Li (38 $\text{mg}\cdot\text{kg}^{-1}$, Table 3) were present in the karst terrain (Mao et al., 2002; Zheng et al., 2013). A new type of carbonate-hosted clay-type Li deposit was recently developed in this terrain and is expected to serve as an important Li source for China (Mao et al., 2019; Wen et al., 2020). The high Li values found in limestone areas was attributed to secondary Li enrichment during

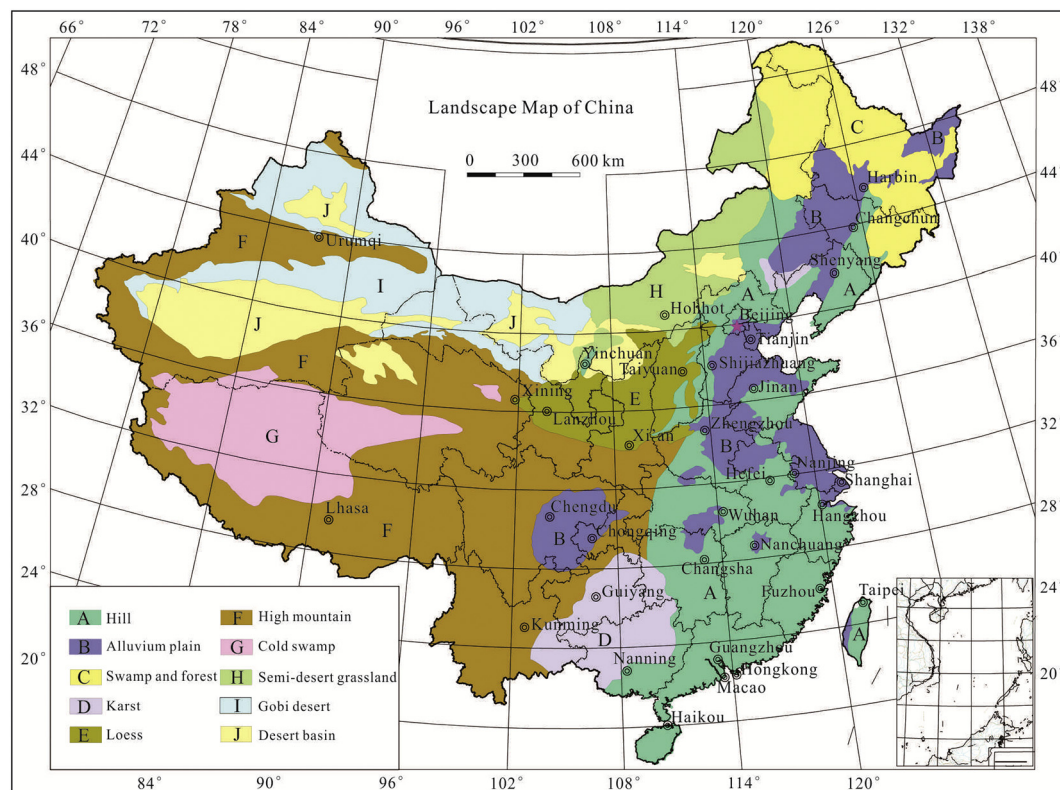


Fig. 4. Outlines of ten geomorphological landscapes in China, modified from Wang et al. (2015).

Table 5
Statistical summary of Li (mg·kg⁻¹) in top and deep catchment sediment samples in China's geomorphological landscapes.

Landscape	Sample type	Num.	Min.	P2.5	P25	P50	P75	P85	P97.5	Max.	AM	GM
China	Top	3394	5.37	11.2	22.7	30.0	37.6	42.9	62.3	400	31.6	28.8
	Deep	3394	5.27	9.55	20.7	28.6	37.5	42.9	63.7	400	30.6	27.4
A	Top	633	5.85	11.1	21.2	30.0	39.9	45.3	65.2	126	31.9	28.8
	Deep	633	5.27	9.78	21.1	29.5	42.5	48.7	69.0	110	32.7	29.0
B	Top	335	6.75	10.5	24.0	30.3	36.6	39.9	51.1	72.5	30.3	28.3
	Deep	335	6.87	9.83	22.6	30.4	38.0	42.3	55.6	70.6	30.7	28.1
C	Top	218	11.4	14.4	25.1	29.8	34.4	37.2	47.5	63.1	30.0	28.8
	Deep	218	8.75	12.1	21.3	27.8	34.4	36.6	47.8	77.5	27.9	26.3
D	Top	126	7.09	13.7	25.1	33.4	40.1	45.6	66.0	181	35.5	32.0
	Deep	126	7.31	16.4	28.3	35.4	42.8	46.4	74.6	127	37.2	34.7
E	Top	170	9.21	12.0	23.7	29.5	33.8	36.4	44.3	62.5	28.8	27.4
	Deep	170	6.91	10.0	21.3	27.3	31.9	35.7	45.0	49.4	27.0	25.4
F	Top	935	7.35	16.7	26.8	32.9	41.1	47.7	70.8	400	36.5	33.6
	Deep	935	7.35	13.5	25.8	32.5	40.4	47.0	72.1	400	35.5	32.4
G	Top	140	13.9	18.0	24.9	30.1	38.2	46.9	68.1	91.3	33.3	31.4
	Deep	140	13.3	17.7	24.9	30.6	37.3	43.2	63.2	91.9	32.8	31.1
H	Top	215	7.82	9.50	15.4	21.3	30.9	36.1	55.2	122	24.6	21.8
	Deep	215	5.42	7.25	13.8	19.8	28.4	35.1	52.5	161	23.3	20.1
I	Top	424	5.37	11.3	19.6	27.0	36.1	40.7	52.9	97.0	28.3	25.9
	Deep	424	5.37	8.95	15.5	21.3	30.1	36.6	49.6	151.4	24.3	21.8
J	Top	198	6.12	7.21	15.8	22.9	30.0	37.0	55.3	61.5	24.6	21.8
	Deep	198	6.19	7.62	15.3	21.4	27.7	32.0	50.7	58.4	22.6	20.3

Notation: Num. = Number of samples; P = Percentile (P50 = Median); Min. = Minimum; Max. = Maximum; AM = Arithmetic mean; GM = Geometric mean; China – all samples; A – Hill; B – Alluvium; C – Swamp and forest; D – Karst; E – Loess; F – High mountain; G – Cold swamp; H – Semi-desert grassland; I – Gobi desert; J – Desert basin.

weathering (Negrel et al., 2017). Those might explain the high median value of Li in the karst landscape.

3.4. Spatial distribution of Li throughout China and geochemical prediction of Li metallogenic belt

Reliable geochemical maps play an important role in mineral exploration and environmental studies (Reimann et al., 2008; Grunsky et al., 2009). Geochemical maps of Li throughout China (Figs. 7 and 8) were drawn using GeoExpl2012 software, which was developed by the Development and Research Center, China Geological Survey (<http://www.drc.cgs.gov.cn/GeoExplGeoMDIS/>). Raw analytical data were interpolated to generate a regular output grid of 80 × 80 km using an exponentially-weighted moving average model (Wang et al., 2015). Eighteen-shade color map classes were set according to the following Li concentration percentiles: P2.5, P5, P10, P15, P20, P25, P30, P40, P50, P60, P70, P75, P80, P85, P90, P95, and P97.5. These were equivalent to 11.2, 13.1, 16.1, 18.7, 20.8, 22.7, 24.1, 27.3, 30.0, 32.5, 35.9, 37.6, 39.8, 42.9, 46.8, 53.6, and 62.3 mg·kg⁻¹ for the top samples, and 9.55, 11.5, 14.3, 16.5, 18.7, 20.7, 22.3, 25.5, 28.6, 31.6, 35.4, 37.5, 39.8, 42.8, 47.4, 54.1, and 63.7 mg kg⁻¹ for the deep samples.

A previous study (Li et al., 2014, 2015) determined 12 Li metallogenic belts according to the distribution of Li mineral deposits (4 super large-scale, 19 large-scale, 20 medium-scale, and 28 small-scale) and the scope of national metallogenic belts and orogenic belts (Table 6 and Fig. 6). These were as follows: hard rock type Li ore resource zones: Altay Li belt, Kangbale Li belt, West Tianshan Li belt, East Tianshan Li belt, West Kunlun Li belt, Songpan-Ganzi Li belt, Qinling Li belt, and South China Li belt; salt lake type Li ore resource zones: North Tibet Li belt, Qaidam Li belt, Sichuan basin Li belt, and Jiangnan basin Li belt (Li et al., 2014, 2015).

Macroscopically, the spatial distribution of Li in the top and deep samples was relatively consistent, which indicates good consistency in the deposition of Li in the catchment sediments of China. The low background area of Li (< P25) was mainly distributed in the northern margin of the North China craton and Hainan Island, and the high background area (> P75) was mainly distributed in the Altay, South China, Sanjiang and Himalayan orogenic belts, and the Yangtze craton (Figs. 7 and 8). The 85th percentile (42.9 mg·kg⁻¹) was set as the anomaly threshold for the top catchment sediment samples. The continuous anomalous point distribution enabled the delineation of 16 geochemical anomalies and eight important prospective Li resources,

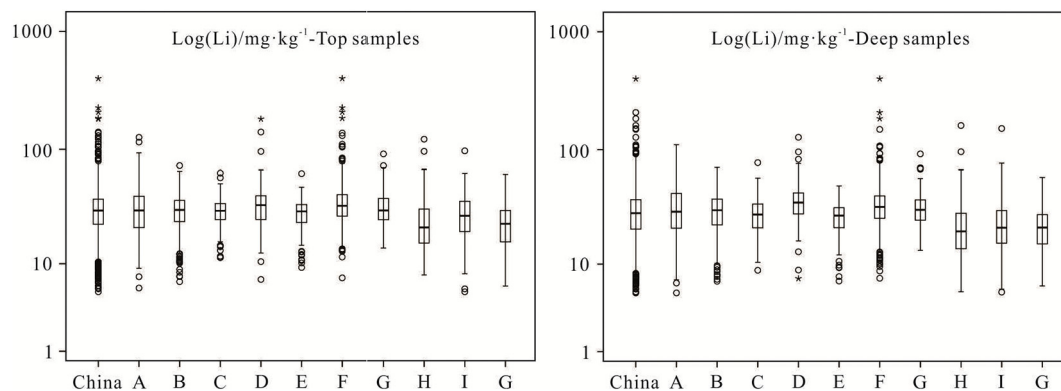


Fig. 5. Boxplots showing the Li (mg·kg⁻¹) variation in the top and deep catchment sediment samples in different geomorphological landscapes of China. Notation: China – all samples; A – Hill; B – Alluvium; C – Swamp and forest; D – Karst; E – Loess; F – High mountain; G – Cold swamp; H – Semi-desert grassland; I – Gobi desert; J – Desert basin.

Table 6
The main Li ore-forming belts and Li deposits of China (After Li et al., 2014, 2015).

Num.	Ore-forming belts	Typical deposits		Tectonic setting
		Name	Mineralization scale	
01	Altay Li belt	Koktokay	Large	Altay orogenic belt
		Kukalagai	Medium	
		Kelumute	Medium	
02	Kangbale Li belt	Heshihaxihali	Small	Junggar block and its peripheral orogenic belt
03	West Tianshan Li belt	Shayintubai	Small	Northeast margin orogenic belt of Yili microplate
04	East Tianshan Li belt	Jingerquan	Small	Jueluotage–Heiyingshan orogenic belt
05	West Kunlun Li belt	Dahongliutan	Medium	West Kunlun orogenic belt
		Aketasi	Medium	
06	North Tibet Li belt	Zabuye	Large	Closed high evaporation environment of the Quaternary
		Dangxiongcuo	Large	
		Laguocuo	Large	
		Mamicuo	Large	
07	Chaidamu Li belt	Longmucuo	Large	Closed high evaporation environment of the Quaternary
		Qarhan	Super-large	
		East Taijinar	Large	
		West Taijinar	Large	
		Yiliping	Large	
08	Songpan-Ganzi Li belt	Gasikule	Large	Songpan–Ganzi orogenic belt
		Dachaidan	Medium	
		Jiajika	Super-large	
		Lijiagou	Super-large	
		Guanyinqiao	Large	
09	Sichuan basin Li belt	Rongxuka	Medium	Depression of Sichuan basin
		Zhawulong	Medium	
		Pingluoba	Medium	
10	Qinling Li belt	Caijiagou	Medium	Qinling orogenic belt
		Nanyangshan	Small	
11	Jianghan basin Li belt	Qianjiang	Large	Jianghan– Dongting fault depression
12	South China Li belt	Yichun	Super-large	South China orogenic belt
		Tongan	Large	
		Jianfengling	Large	
		Zhengchong	Large	
		Xikeng	Large	
		Chuanziyuan	Medium	
		Qiuzhuke	Small	

which roughly corresponded to the Li metallogenic belts defined by Li et al. (2014). However, individual salt lake sediments were not sampled during the CGB project, which resulted in non-obvious anomalies in some salt lake type Li resource areas. For example, the Qarhan salt lake (Fig. 6) exhibited only a weak anomaly. Additionally, some remote areas in Northern Tibet were not sampled, resulting in the failure to completely cover the Li belt in North Tibet and the appearance of geochemical anomalies only in the periphery of the Li belt. Eight geochemical Li belts were identified as important prospective Li resources (Fig. 7): South China (Li11), South Tibet (Li05), Kunming-Guiyang-Xiangxi (Li08), western Sichuan (Jiajika, Li06), Dahongliutan (Li03), Sanjiang (Li07), Bianba-Nangqian (Li04) and Altay (Li01).

Elemental distribution patterns in continental-scale geochemical maps are mainly determined by natural variations (Reimann et al., 2009). The principal Li anomalies were spatially associated with granitic rocks and Li-pegmatites and their weathering products (Negrel et al., 2017). In areas Li11, Li05, Li06, Li03, Li07, and Li01 in Fig. 7, outcropped granitic rocks were the main contributors. This explains the extensive anomalous Li concentrations in the South China, Tibet-

Sanjiang, Songpan-Ganzi and Altay orogen belts where large-scale magmatic activities occurred. To further study the influence of the geological background on Li concentration, spots representing different Li concentrations and granite outlines are shown in Fig. 9, which showed that high Li concentrations closely matched the granite distribution. After the emplacement of these granites, many world-renowned Li mineralizations were produced, such as the Mufushan ore field which is located at the junction of Hubei, Hunan, and Jiangxi provinces and is rich in rare metals, non-ferrous metals, precious metals, and uranium (Li et al., 2020); Yichun 414, Jianfengling, Tongan, Zhengchong, and Xikeng deposits were formed in Li11, the Jiajika, Lijiagou, Ke'eryin and Guanyinqiao deposits were formed in Li06, the Dahongliutan and Aketasi deposits were formed in Li03, and the Koktokay, Kukalagai, and Kelumute deposits were formed in Li01 (Table 6, Figs. 6 and 7). They are well delineated in the geochemical anomalies in both top and deep samples (Figs. 7 and 8). It should be pointed out that Li05 is not only related to the leucogranites widely developed in the Gangdese orogen, but also to the salt lakes rich in Li, such as Zabuye, Dangxiongcuo, Laguocuo, Mamicuo, Longmucuo (Table 6, Figs. 6 and 7). Those salt lakes are in geologically recent enclosed basins that contain lacustrine evaporites produced due to high rates of evaporation relative to precipitation (Kesler et al., 2012). A high-Li band (Li08, Fig. 7) was present in the Yangtze craton, which may be related to black shales and is located in the karst landscape. The clay rocks enriched in Li primarily included the Jiujialu formation in the lower Carboniferous in the Guizhou Province and the Daoshitou formation in the lower Permian in central Yunnan Province. A new type of carbonate-hosted clay-type Li deposit was defined by Wen et al. (2020): 1) ore-forming materials are derived from the underlying carbonate formation; 2) lithium mainly exists in the smectite phase due to adsorption; and 3) the sedimentary environment plays an important role in Li enrichment, which is expected to become an important Li source in China (Mao et al., 2019; Wen et al., 2020). The concentration and distribution of Li in soils (sediments) are controlled by the parent rock and are also related to the soil properties, especially the clay content (Lavado et al., 1978; Kashin, 2019). Table 7 shows the correlation between Li and Al_2O_3 , TFe_2O_3 , MgO, MnO, C_{org} , K_2O , CaO, SiO_2 , Na_2O based on the CGB data. There were strong positive correlations between Li and Al_2O_3 , TFe_2O_3 , MgO, MnO and C_{org} and a strong negative correlation between Li and SiO_2 . Soils inherit their Li content from the underlying indigenous rock. As a result of the weathering of parent rocks, Li is relatively easily released from primary minerals, passed into moving forms, and finally accumulated in clay minerals. The accumulation and distribution of Li in soils is influenced by the humus content and composition of clay minerals (Sobolev et al., 2019).

3.5. Lithium distribution relationship to acidic rock

Rock samples were simultaneously collected during the CGB project to interpret the geogenic sources of sediment geochemical patterns (Wang et al., 2015; Han, 2019). Lithium resources were mainly related to acidic rocks such as granite, granitic pegmatite, and their hydrothermal fluids (Li et al., 2014, 2015). To further investigate the relationship between the geochemical distribution pattern of Li in sediments and the geological background (granitoids), a total of 2077 acidic rock samples were collected from exposed bedrock during the CGB project.

Table 8 shows the statistical results of Li concentrations in acidic rock samples of China. The Li concentration range was $0.73\text{--}476\text{ mg}\cdot\text{kg}^{-1}$, and the median value was $18.5\text{ mg}\cdot\text{kg}^{-1}$, which was nearly half of that in the top catchment sediment samples. These findings revealed that Li was enriched from the rock to sediment, possibly due to weathering during soil formation. Lithium was released from primary silicate minerals and then proportionally incorporated with aluminum into secondary clays during pedogenesis. Lithium was retained because its ionic radius was well matched to the octahedral



Fig. 6. The distribution of Li metallogenic belts and major lithium deposits in China (redrawn from Li et al., 2014, 2015).

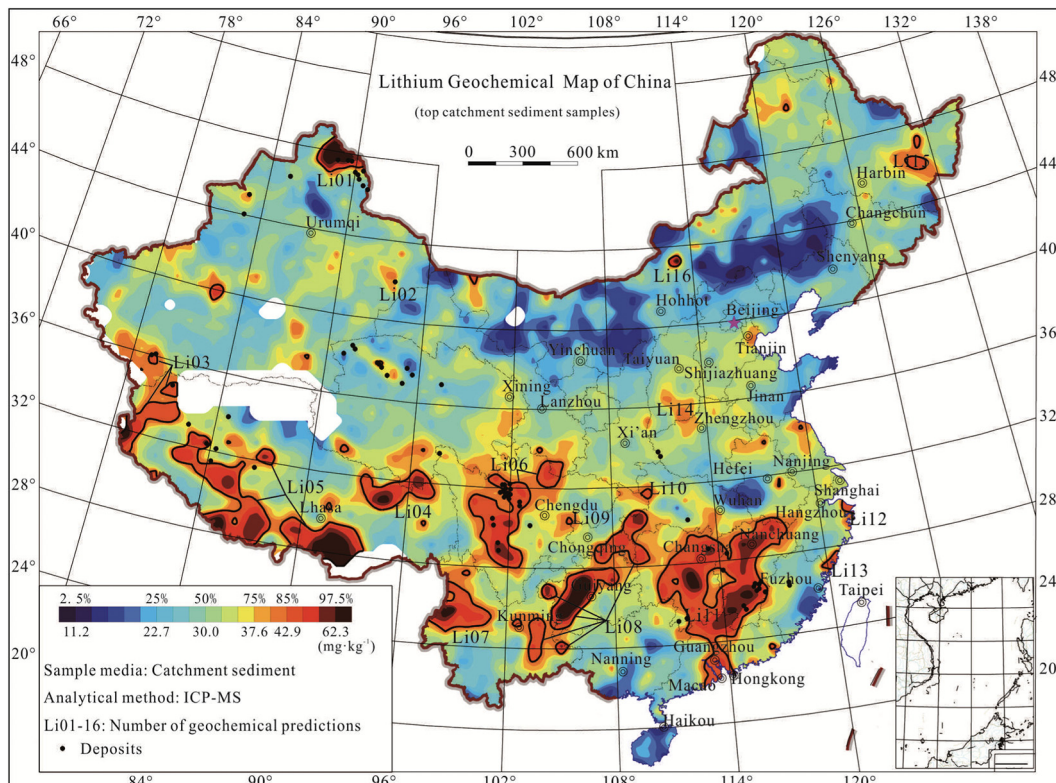


Fig. 7. Li distribution map in the top catchment sediment samples from the CGB project.

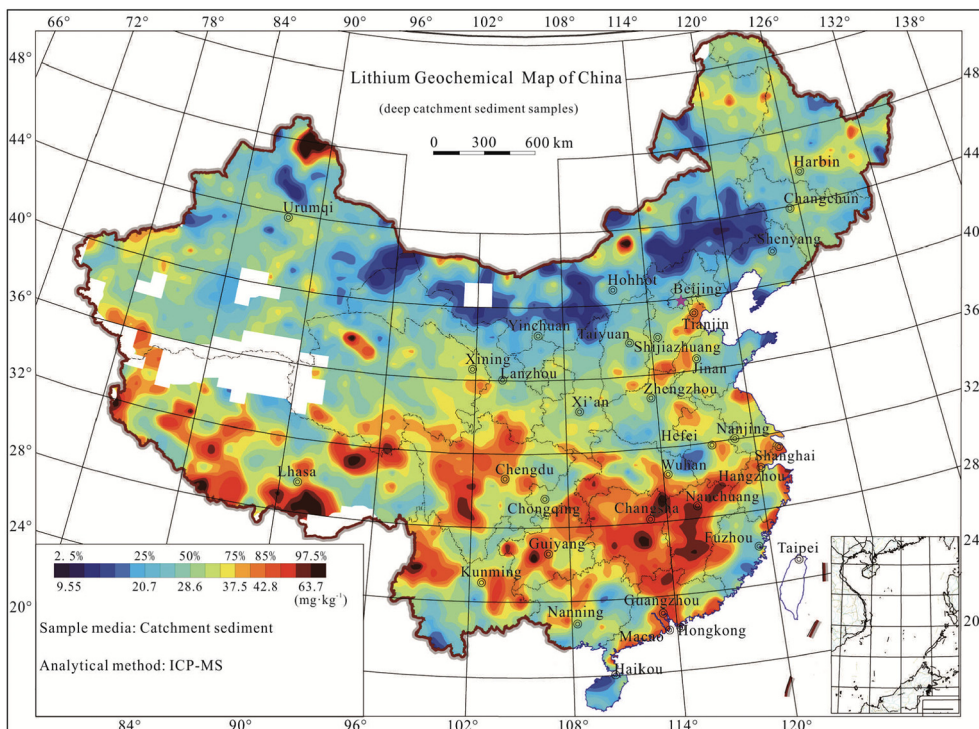


Fig. 8. Li distribution map in the deep catchment sediment samples from the CGB project.

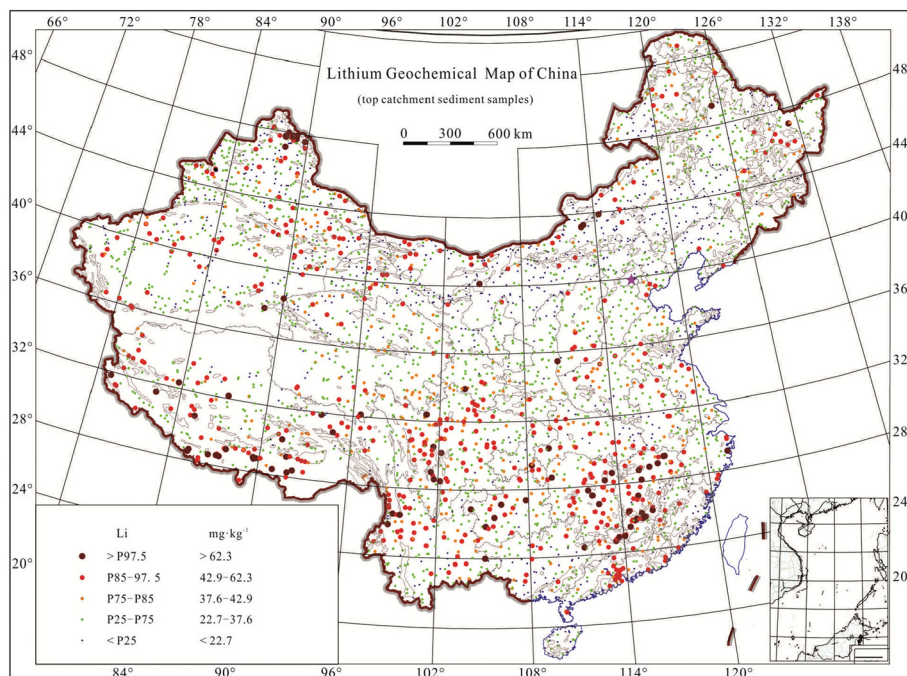


Fig. 9. Map of Li concentrations in top catchment sediment samples of the CGB project and granite distribution in China.

Table 7

Correlation analysis (R) between Li and Al₂O₃, TFe₂O₃, MgO, MnO, C_{org}, K₂O, CaO, SiO₂, Na₂O in the top and deep samples.

Li	Al ₂ O ₃	TFe ₂ O ₃	MgO	MnO	C _{org}	K ₂ O	CaO	SiO ₂	Na ₂ O
Top samples	0.456	0.471	0.226	0.224	0.210	0.100	0.038	-0.373	-0.130
Deep samples	0.455	0.469	0.217	0.260	0.245	0.048	0.031	-0.421	-0.165

Table 8
The statistical parameters of the Li concentration ($\text{mg}\cdot\text{kg}^{-1}$) in acidic rocks of China.

Tectonic unit	Num.	Min.	P2.5	P25	P50	P75	P85	P97.5	Max.	AM	GM
China	2077	0.73	2.47	9.72	18.5	31.8	43.3	100	476	26.3	17.4
I	736	0.73	2.53	8.67	16.4	27.0	33.8	61.2	147	20.1	14.8
II	413	1.13	2.54	7.78	13.4	22.3	28.5	62.0	196	18.1	13.0
VI	244	1.20	2.07	10.7	22.0	33.6	42.7	149	322	29.3	17.9
III	96	1.50	1.75	10.6	20.3	44.2	68.0	238	345	42.7	20.7
VII	388	0.96	3.72	13.9	25.8	47.5	62.7	111	476	36.3	24.5
VIII	30	2.15	2.55	12.1	20.2	26.7	30.2	61.9	74.0	21.9	15.7
IV	48	3.42	3.76	13.7	31.6	67.1	83.5	155	244	45.5	28.7
V	122	3.49	7.84	20.3	31.1	44.2	52.6	104	156	35.3	29.0

Notation: Num. = Number of samples; P = Percentile (P50 = Median); Min. = Minimum; Max. = Maximum; AM = Arithmetical mean; GM = Geometric mean; China – all samples; I – Tianshan-Xingmeng orogenic belt; II – North China craton; III – Qin-Qi-Kun orogenic belt; IV – Yangtze craton; V – South China orogenic belt; VI – Tarim craton; VII – Songpan-Ganzi orogenic belt; VIII – Tibet-Sanjiang orogenic belt.

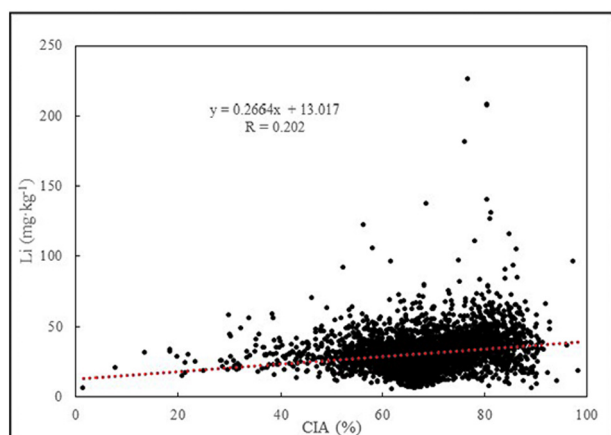


Fig. 10. Scatterplot of Li concentration vs. CIA.

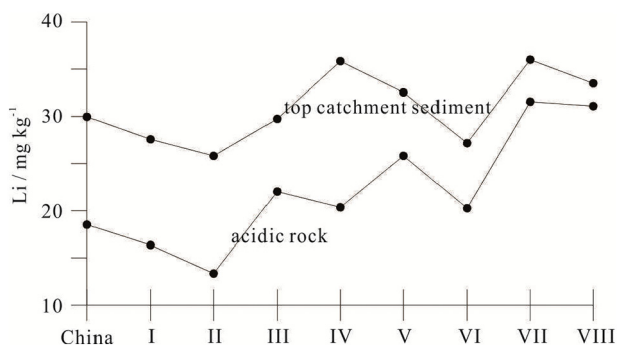


Fig. 11. The variation in Li median concentrations in top catchment sediment samples and acidic rock samples in various tectonic belts of China. Notation: China – All samples; I – Tianshan-Xingmeng orogenic belt; II – North China craton; III – Qin-Qi-Kun orogenic belt; IV – Yangtze craton; V – South China orogenic belt; VI – Tarim craton; VII – Songpan-Ganzi orogenic belt; VIII – Tibet-Sanjiang orogenic belt.

cavity of clay minerals (Huh et al., 2004; Tsai et al., 2014). The chemical index of alteration (CIA) is widely used to indicate the degree of weathering of source areas (Kasanzu et al., 2008; Négrel et al., 2015). The CGB project evaluated the weathering history of top samples using the CIA, defined by Nesbitt and Young (1982) as: $CIA = \frac{[mAl_2O_3 / (mAl_2O_3 + mCaO + mNa_2O + mK_2O)] \times 100}$. According to the scatter plot in Fig. 10, the Li concentration was linearly related to the CIA, indicating that weathering or soil formation enrich Li in soils.

Fig. 11 shows variations in the median Li concentrations in the top catchment sediments and acidic rocks in various tectonic belts of China (Fig. 11). In these samples, the highest Li concentrations were found in the Songpan-Ganzi, Tibet-Sanjiang and South China orogenic belts and

the Yangtze craton, which all showed virtually identical variation trends. The spatial distribution of the correlation between Li concentration in the top catchment sediment and acidic rock samples is shown in Fig. 12. The high Li concentrations in the top samples closely matched those in the acidic rock samples, which indicates that the Li concentration in catchment sediments was constrained by the Li concentration in acidic rocks in various tectonic belts of China.

4. Conclusions

The China Geochemical Baselines project, based on catchment sediment sampling, provided the first continental-scale geochemical survey of the general abundance and distribution of Li throughout China. The range of Li concentrations in the top catchment sediment samples was $5.37\text{--}400\text{ mg}\cdot\text{kg}^{-1}$ with a median of $30.0\text{ mg}\cdot\text{kg}^{-1}$, and the range of Li concentrations in the deep catchment sediment samples was $5.27\text{--}400\text{ mg}\cdot\text{kg}^{-1}$ with a median of $28.6\text{ mg}\cdot\text{kg}^{-1}$. The Li concentrations in the top and deep catchment sediments of China greatly varied across regions, but only mildly varied across profiles. Parent rock, predominantly governed the Li distribution in the catchment sediments of China, while landscapes, mineralization, and weathering played regional-scale roles. Based on the 85th percentile of Li concentrations in the top catchment sediment samples, a total of 16 geochemical anomalies were delineated, and eight important prospective Li resources were identified. The high-Li area was mainly distributed in the Altay, South China, Sanjiang and Himalayan orogenic belts, and the Yangtze craton, where many world-renowned Li deposits were formed.

CRedit authorship contribution statement

Hanliang Liu: Conceptualization, Software, Formal analysis, Investigation, Data curation, Writing - original draft, Writing - review & editing. **Xueqiu Wang:** Conceptualization, Writing - original draft, Writing - review & editing, Supervision, Project administration, Funding acquisition. **Bimin Zhang:** Investigation, Data curation, Writing - review & editing. **Wei Wang:** Investigation, Software, Data curation. **Zhixuan Han:** Investigation, Data curation, Writing - review & editing. **Qinghua Chi:** Investigation, Data curation. **Jian Zhou:** Investigation, Data curation. **Lanshi Nie:** Investigation, Software, Data curation. **Shanfa Xu:** Investigation, Data curation. **Wensheng Yao:** Investigation, Data curation. **Dongsheng Liu:** Investigation, Data curation. **Qingqing Liu:** Investigation, Data curation. **Jian Liu:** Writing - review & editing.

Declaration of competing interest

The authors declared that they have no conflicts of interest to this work.

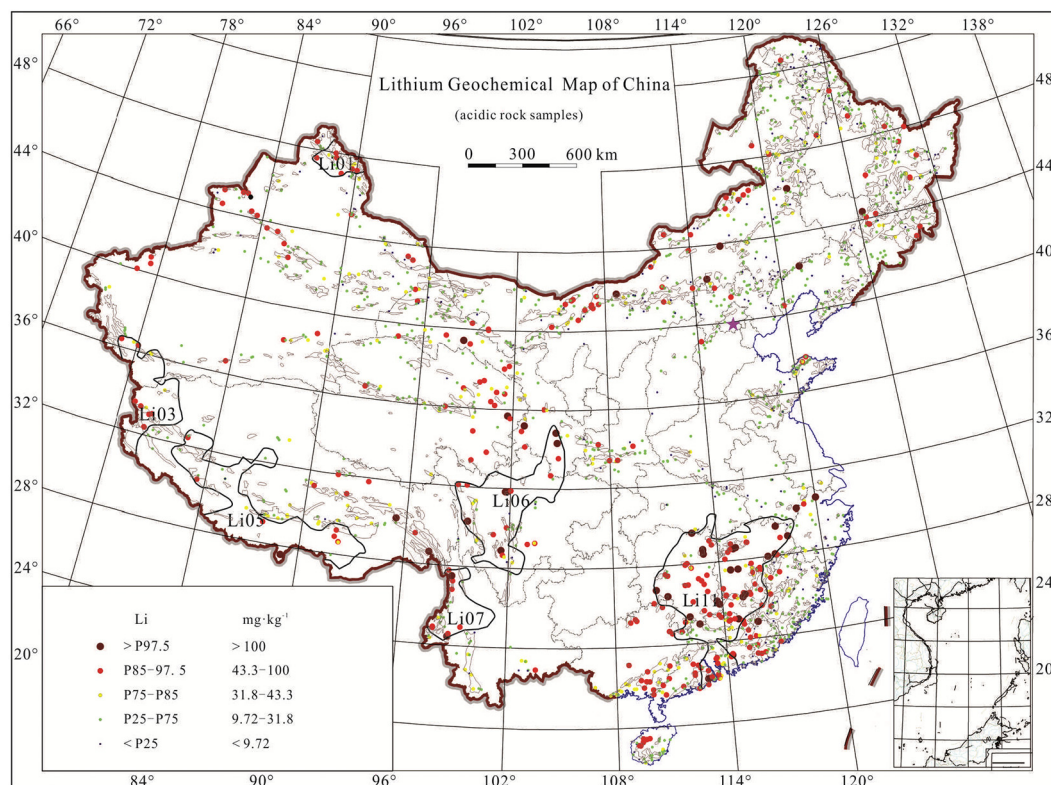


Fig. 12. Map of Li concentrations in acidic rock samples of the CGB project, and granite distribution in China, The black line is an outline of the main Li anomaly based on Fig. 7.

Acknowledgments

Many thanks are given to all participants in the China Geochemical Baselines project for their hard work in field sampling, laboratory analysis and data processing. The constructive comments and suggestions of anonymous reviewers made this paper more readable and robust. This research was supported by the

National Key Research and Development Program of China (2016YFC0600600), National Natural Science Foundation of China (41903071), National Nonprofit Institute Research Grant of IGGE (AS2019P02), the China Geological Survey Project (DD20160116, DD20190450, DD20190451), and the Science and Technology Foundation of MLR, China (Sino-probe-04).

References

- Anderson, M.A., Bertsch, P.M., Miller, W.P., 1988. The distribution of lithium in selected soils and surface waters of the southeastern U.S.A. *Appl. Geochem.* 3, 205–212.
- Ashry, M.M., 1973. Occurrence of Li, B, Cu, and Zn in some Egyptian Nile sediments. *Geochim. Cosmochim. Acta* 37, 2449–2458.
- Caritat, P.d., Cooper, M., Lech, M., McPherson, A., Thun, C., 2009. National Geochemical Survey of Australia: Sample Preparation Manual. Geoscience Australia, pp. 1–28 Record 2009/08.
- Caritat, P.d., Reimann, C., Smith, D.B., Wang, X.Q., 2018. Chemical elements in the environment: Multi-element geochemical datasets from continental- to national-scale surveys on four continents. *Appl. Geochem.* 89, 150–159.
- Chi, Q.H., Yan, M.C., 2007. Handbook of Elemental Abundance for Applied Geochemistry. Geological Publishing House, Beijing (in Chinese).
- CNEMC (China National Environment Monitoring Center), 1990. Soil Element Background Value in China. China Environment Science Press, Beijing (in Chinese).
- Darnley, A.G., Björklund, A., Bølviken, B., Gustavsson, N., Koval, P.V., Plant, J.A., Steenfelt, A., Tauchid, M., Xie, X.J., Garrett, R.G., Hall, G.E.M., 1995. A global geochemical database for environmental and resource management: Final report of IGCP Project 259. In: *Earth Sciences*. 19. UNESCO Publishing, Paris, pp. 122.
- Gil-Alana, L.A., Monge, M., 2019. Lithium: production and estimated consumption. Evidence of persistence. *Resources Policy* 60, 198–202.
- Grunsky, E.C., Drew, L.J., Sutphin, D.M., 2009. Process recognition in multi-element soil and stream sediment geochemical data. *Appl. Geochem.* 24, 1602–1616.
- Han, Z.X., 2019. Abundance and Distribution of Lead in Outcropping Rocks and Catchment Sediments in Mainland China. China University of Geosciences (Beijing), Beijing.
- Huh, Y., Chan, L.H., Chadwick, O.A., 2004. Behavior of lithium and its isotopes during weathering of Hawaiian basalt. *Geochemistry Geophysics. Geosystems*. 5, Q09002.
- Jaskula, B.W., 2017. Mineral commodity summaries—lithium 2017. In: U.S. Geological Survey, . <https://minerals.usgs.gov/minerals/pubs/commodity/lithium/>.
- Kasanzu, C., Maboko, M.A.H., Many, S., 2008. Geochemistry of fine-grained clastic sedimentary rocks of the Neoproterozoic Ikorongo Group, NE Tanzania: Implications for provenance and source rock weathering. *Precambrian Res.* 164, 201–213.
- Kashin, V.K., 2019. Lithium in soils and plants of Western Transbaikalia. *Eurasian Soil Science* 52 (4), 359–369.
- Kesler, S.E., Gruber, P.W., Medina, P.A., Keoleian, G.A., Everson, M.P., Wallington, T.J., 2012. Global lithium resources: relative importance of pegmatite, brine and other deposits. *Ore Geol. Rev.* 48, 55–69.
- Lavado, R.S., González Quintana, J.A., Hevia, G.G., 1978. Content and distribution of lithium in La Pampa soils (Argentina). *Commun. Soil Sci. Plant Anal.* 9 (4), 299–310.
- Li, J.K., Liu, X.F., Wang, D.H., 2014. The metallogenetic of lithium deposits in China. *Acta Geol. Sin.* 88 (12), 2269–2283 (in Chinese with English abstract).
- Li, J.K., Zou, T.R., Liu, X.F., Wang, D.H., Ding, X., 2015. The metallogenetic regularities of lithium deposits in China. *Acta Geologica Sinica (English Edition)* 89 (2), 652–670.
- Li, P., Li, J.K., Liu, X., Li, C., Huang, Z.B., Zhou, F.C., 2020. Geochronology and source of the rare-metal pegmatite in the Mufushan area of the Jiangnan orogenic belt: a case study of the giant Renli Nb-Ta deposit in Hunan, China. *Ore Geol. Rev.* 116, 103237.
- Lin, X., Wang, X.Q., Zhou, J., Chi, Q.H., Nie, L.S., Zhang, B.M., Xu, S.F., Zhao, S.D., Liu, H.L., Sun, B.B., Han, Z.X., Liu, D.S., Wang, W., Liu, Q.Q., Bai, J.F., Fan, H., Ma, N., Zhang, L.S., Xu, G.Z., Wei, W.T., Zhao, B., Shen, W.J., 2019. Concentrations, variations and distribution of molybdenum (Mo) in catchment outlet sediments of China: Conclusions from the China geochemical baselines project. *Appl. Geochem.* 103, 50–58.
- Ma, Z., Li, J.W., 2018. Analysis of China's lithium resources supply system: status, issues and suggestions. *China Mining Magazine* 27 (10), 1–7 (in Chinese with English abstract).
- Mao, J.W., Lehmann, B., Du, A.D., Zhang, G.D., Ma, D.S., Wang, Y.T., Zeng, M.G., Kerrich, R., 2002. Re-Os dates of polymetallic Ni-Mo-PGE-Au mineralization in lower Cambrian black shales of South China and its geologic significance. *Econ. Geol.* 97, 1051–1061.
- Mao, J.W., Yuan, S.D., Xie, G.Q., Song, S.W., Zhou, Q., Gao, Y.B., Liu, X., Fu, X.F., Cao, J., Zeng, Z.L., Li, T.G., Fan, X.Y., 2019. New advances on metallogenetic studies and exploration on critical minerals of China in 21st century. *Mineral Deposits* 38 (5), 935–969 (in Chinese with English abstract).
- Négre, P., Sadeghi, M., Ladenberger, A., Reimann, C., Manfred, B., the GEMAS Project Team, 2015. Geochemical fingerprinting and source discrimination of agricultural soils at continental scale. *Chem. Geol.* 396, 1–15.
- Négre, P., Reimann, C., Ladenberger, A., Birke, M., 2017. Distribution of lithium in

- agricultural and grazing land soils at European continental scale (GEMAS project). EGU General Assembly Abstracts 19, 15340.
- Nesbitt, H.W., Young, G.M., 1982. Early Proterozoic climates and plate motion inferred from major element chemistry of lutites. *Nature* 299, 715–717.
- Reimann, C., Arnoldussen, A., Englaier, P., Filzmoser, P., Finne, T.E., Garrett, R.G., Koller, F., Nordgulen, O., 2007. Element concentrations and variations along a 120 km transect in southern Norway—anthropogenic vs. geogenic vs. biogenic element sources and cycles. *Appl. Geochem.* 22, 851–871.
- Reimann, C., Filzmoser, P., Garrett, R.G., Dutter, R., 2008. *Statistical Data Analysis Explained: Applied Environmental Statistics with R*. John Wiley and Sons Ltd, Chichester, pp. 53–55.
- Reimann, C., Matschullat, J., Birke, M., Salminen, R., 2009. Arsenic distribution in the environment: the effects of scale. *Appl. Geochem.* 24, 1147–1167.
- Reimann, C., Caritat, P.d., GEMAS Project Team, NGS Project Team, 2012. New soil composition data for Europe and Australia: demonstrating comparability, identifying continental-scale processes and learning lessons for global geochemical mapping. *Sci. Total Environ.* 416, 239–252.
- Ren, J.S., Wang, Z.X., Chen, B.W., Jiang, C.F., Niu, B.G., Li, J.Y., Xie, G.L., He, Z.J., Liu, Z.G., 1999. *The Tectonics of China from a Global View—a Guide to the Tectonic Map of China and Adjacent Regions*. Geological Publishing House, Beijing, pp. 32 (in Chinese).
- Rudnick, R.L., Gao, S., 2003. The composition of the continental crust. In: Holland, H.D., Condie, K. (Eds.), *The Crust. Treatise on Geochemistry*, vol. 3. Elsevier Pergamon, Amsterdam, pp. 1–64.
- Salminen, R., Tarvainen, T., 1997. The problem of defining geochemical baselines. A case study of selected elements and geological materials in Finland. *J. Geochem. Explor.* 60, 91–98.
- Shi, C.Y., Yan, M.C., Liu, C., Chi, Q.H., Hu, S.Q., Gu, T.X., et al., 2005. Abundances of chemical elements in granitoids of China and their characteristics. *Geochimica* 34 (5), 470–482 (in Chinese with English abstract).
- Smith, D.B., Wang, X.Q., Reeder, S., Demetriades, A., 2012. The IUGS/IAGC task group on global geochemical baselines. *Earth Science Frontiers* 19 (30), 1–6.
- Sobolev, O.I., Gutjy, B.V., Darmohray, L.M., Sobolieva, S.V., Ivanina, V.V., Kuzmenko, O.A., Karkach, P.M., Fesenko, V.F., Bilkevych, V.V., Mashkin, Y.O., Trofymchuk, A.M., Stavetska, R.V., Tkachenko, S.V., Babenko, O.I., Klopenko, N.I., Chernyuk, S.V., 2019. Lithium in the natural environment and its migration in the trophic chain. *Ukrainian Journal of Ecology* 9 (2), 195–203.
- Taylor, S.R., 1964. The abundance of chemical elements in the continental crust: a new table. *Geochim. Cosmochim. Acta* 28, 1273–1285.
- Taylor, S.R., McLennan, S.M., 1985. *The Continental Crust: Its Composition and Evolution*. Blackwell Scientific Publications, London, pp. 312.
- Tsai, P.H., You, C.F., Huang, K.F., Chung, C.H., Sun, Y.B., 2014. Lithium distribution and isotopic fractionation during chemical weathering and soil formation in a loess profile. *J. Asian Earth Sci.* 87, 1–10.
- Wang, X.Q., 2012. Global geochemical baselines: understanding the past and predicting the future. *Earth Science Frontiers* 19 (3), 7–18 (in Chinese with English abstract).
- Wang, J.A., Zuo, W., 2010. *Geographic Atlas of China*. Sinomaps, Beijing (in Chinese). *Geographic Atlas of China*. Sinomaps, Beijing (in Chinese).
- Wang, X.Q., the CGB Sampling Team, 2015. China geochemical baselines: Sampling methodology. *J. Geochem. Explor.* 148, 25–39.
- Wang, X.Q., Liu, X.M., Han, Z.X., Zhou, J., Xu, S.F., Zhang, Q., Chen, H.J., Bo, W., Xing, X., 2015. Concentration and distribution of mercury in drainage catchment sediment and alluvial soil of China. *J. Geochem. Explor.* 154, 32–48.
- Wang, X.Q., Han, Z.X., Wang, W., Zhang, B.M., Wu, H., Nie, L.S., Zhou, J., Chi, Q.H., Xu, S.F., Liu, H.L., Liu, D.S., Liu, Q.Q., 2019. Continental-scale geochemical survey of lead (Pb) in mainland China's pedosphere: Concentration, spatial distribution and influences. *Appl. Geochem.* 100, 55–63.
- Wedepohl, K.H., 1995. The composition of the continental crust. *Geochim. Cosmochim. Acta* 59, 1217–1232.
- Wen, H.J., Luo, C.G., Du, S.J., Yu, W.X., Gu, H.N., Ling, K.Y., Cui, Y., Li, Y., Yang, J.H., 2020. Carbonate-hosted clay-type lithium deposit and its prospecting significance. *Chin. Sci. Bull.* 65, 53–59 (in Chinese with English abstract).
- Xie, X.J., Cheng, H.X., 1997. The suitability of floodplain sediment as a global sampling medium: evidence from China. *J. Geochem. Explor.* 58, 51–62.
- Xie, X.J., Cheng, H.X., 2001. Global geochemical mapping and its implementation in the Asia-Pacific region. *Appl. Geochem.* 16, 1309–1321.
- Yan, M.C., Chi, Q.H., 2005. *The Chemical Composition of the Continental Crust and Rocks in the Eastern Part of China*. Science Press, Beijing, pp. 171.
- Zhang, Q., Bai, J.F., Wang, Y., 2012. Analytical scheme and quality monitoring system for China Geochemical Baselines. *Earth Science Frontiers* 19 (3), 33–42 (in Chinese with English abstract).
- Zheng, Y.F., Xiao, W.J., Zhao, G.C., 2013. Introduction to tectonics of China. *Gondwana Res.* 23 (4), 1189–1206.